Applied Physics Letters

Effects of phase delay on synchronization in a nonlinear micromechanical oscillator

Cite as: Appl. Phys. Lett. **114**, 233501 (2019); https://doi.org/10.1063/1.5090977
Submitted: 31 January 2019 . Accepted: 25 May 2019 . Published Online: 10 June 2019

Ronghua Huan, Dong Pu, Xuefeng Wang, and Xueyong Wei

Effects of phase delay on synchronization in a nonlinear micromechanical oscillator

Cite as: Appl. Phys. Lett. **114**, 233501 (2019); doi: 10.1063/1.5090977
Submitted: 31 January 2019 · Accepted: 25 May 2019 ·
Published Online: 10 June 2019

View Online Export Citation CrossMark

Ronghua Huan,[1,a)] Dong Pu,[1,2,a)] Xuefeng Wang,[1,2] and Xueyong Wei[2,3,b)]

AFFILIATIONS

[1]Department of Mechanics, Key Laboratory of Soft Machines and Smart Devices of Zhejiang Province, Zhejiang University, Hangzhou 310027, China
[2]State Key Laboratory for Manufacturing Systems Engineering, Xi'an Jiaotong University, Xi'an 710049, China
[3]State Key Laboratory of Applied Optics, Changchun Institute of Optics, Fine Mechanics and Physics, Chinese Academy of Sciences, Changchun 130033, China

[a)]**Contributions:** R. Huan and D. Pu contributed equally to this work.
[b)]**Electronic mail:** seanwei@mail.xjtu.edu.cn

ABSTRACT

Phase feedback is commonly utilized to set up a MEMS oscillator. In most studies, the phase delay is fixed on $\pi/2$ for a maximum oscillation amplitude. In this letter, we study the dynamics of synchronization in a nonlinear micromechanical oscillator operating on different phase delays. The analytical and experimental results show that the synchronization region shifts and the size of this region varies depending on the phase delay. The frequency stability of the self-sustained oscillator holds the best in the case of phase delay equal to $\pi/2$ and can be further improved to the same level after synchronization. Our work reveals the effects of phase delay on synchronization and presents an easy-to-implement strategy for tuning the synchronization by controlling the phase delay of the oscillation feedback circuit in a nonlinear micromechanical oscillator.

Micro/nanomechanical oscillators[1,2] have been widely used in frequency-shift based sensors[3] due to their advantages of low power consumption and easy miniaturization and integration with electronics and have currently become potential alternatives as the frequency reference for timing[4] to quartz-crystal based oscillators which is always kept in the linear regime and requires high carrier power to suppress phase noise.[5] Due to the size effect,[6] micro/nanoresonators are easier to be excited into the nonlinear regime[7] with performance degradation.[8,9]

Efforts have been invested to circumvent these defects to improve the frequency stability and reduce the phase noise using the synchronization phenomenon,[10,11] which is a ubiquitous phenomenon[12] first found by Huygens in coupled pendulums[13] and conventionally defined as an adjustment of rhythms of oscillators in the presence of weak coupling.[14] When two identical micromechanical oscillators are electrically synchronized, their frequency stability can be improved up to sevenfold.[15] Previous studies show that the frequency stability can be improved nearly tenfold at 2 s (integration time) and can be further improved by a larger perturbation,[16] and even in high order synchronization (3:1), improvements can be observed as well.[17] Two anharmonic nanomechanical oscillators suppress the phase noise up to half in the phase synchronized state.[18] In addition, synchronization has shown its potential for mass sensing applications in oscillation arrays by enhancing the frequency stability.[19] However, due to micromachining error, the synchronous state of independently running oscillators faces difficulties owing to its narrow synchronization region and limited tuning approach, especially in high order synchronization.[20,21] In classic models, the synchronization region is tiny and proportional to the perturbation.[22] Research studies have been conducted to clarify the significant role nonlinearity played in enhancing the synchronization region.[23,24] Extra frequency tuning approaches are employed to compensate the frequency detuning to form synchronization, i.e., electrostatic softening spring effect,[15] amplitude-frequency effect,[20] and piezoresisitive effect.[17] A suitable synchronization region (the location of synchronizing frequency and the size of the synchronization region) will make synchronization easy to achieve and applicable for a variety of fields.

To address this problem, we present a strategy for tuning the synchronization using phase delay within the feedback loop, which is easy to implement. In the aforementioned studies, phase feedback is commonly used together with micro/nano electro mechanical system (M/NEMS) resonators to setup the oscillators[25] which meanwhile are essential components[14] in these synchronization processes. Both theoretically[21,26] and experimentally,[15–17,23] the phase delay is shifted to $\pi/2$ for a maximum amplitude with a high signal to noise ratio while its effects on synchronization in nonlinear nano/micromechanical oscillators have not been studied yet.

In this letter, a phase feedback oscillator is implemented combining a micromechanical resonator working in its nonlinear regime with a phase feedback sustaining circuit with a tunable phase delay. We study the effects of phase delay on the synchronization region both analytically and experimentally. The micromechanical clamped to clamped (C-C) beam resonator is fabricated by a standard Silicon-On-Insulator (SOI) process, whose dimensions are 478 μm long, 10 μm wide, and 25 μm thick, respectively. It is electrically actuated and sensed embedded in an electrical circuit with a digital locked-in amplifier (LIA) HF2LI shown in Fig. 1(a). The motional response is preamplified by a transimpedance amplifier (TIA) and filtered by a low-pass filter (LPF) before being loaded to the input port of LIA. Figure 1(b) shows a finite element method (FEM) simulation of the resonator which operates in its principle flexural mode. The device is tested in a vacuum chamber at a pressure below 2 Pa at room temperature. The measured quality factor Q ≈ 18 000, while V_{ac} equals 10 mv [Fig. 1(c)]. The open loop responses of the resonator are obtained with built-in phase-locked loop (PLL) off, and the self-sustained oscillation is setup when PLL is on. The frequency outputs are logged by a frequency counter.

The open loop responses of the resonator, actuated by a combination of a fixed Vdc value (15 V) with various V_{ac} values (perturbation off), are shown in Fig. 2. The comb fingers can linearly drive the resonator for a large amplitude with the limited electrostatic softening effect. The motion for this forced nonlinear micromechanical beam is described using the Duffing equation[27]

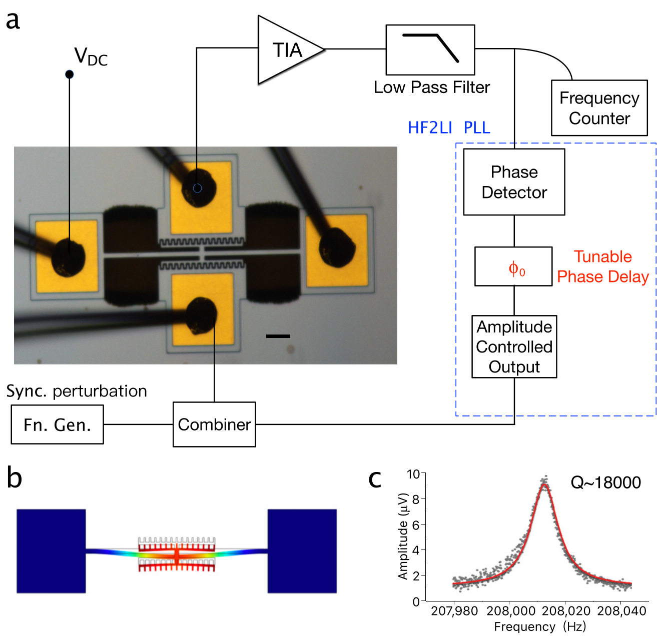

FIG. 1. (a) Schematic graph of the experimental setup. The black scale bar is 50 μm. (b) Structure of the beam microresonator and modal shape simulation in COMSOL. (c) Linear frequency response of the resonator. The measured quality factor Q ≈ 18 000 while the resonator responses linearly under weak excitation (V_{ac} = 10 mV). The red line is the Lorentzian fitting curve.

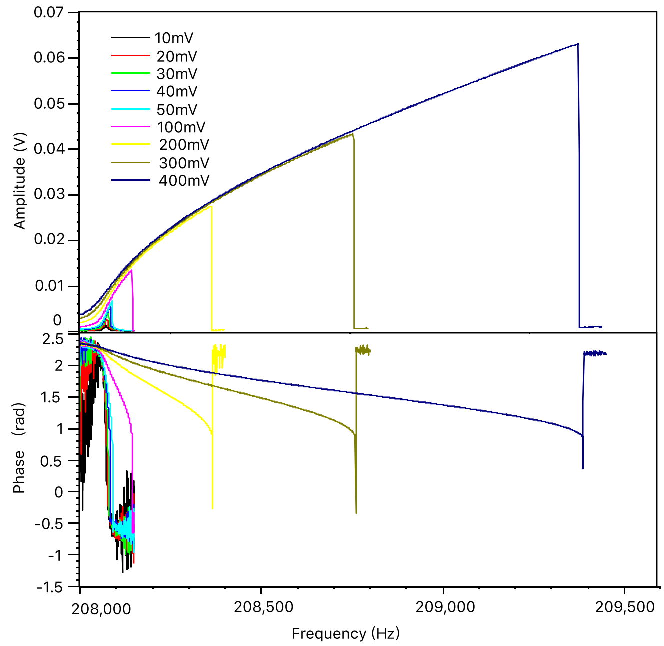

FIG. 2. Open loop characterization of the resonator on various V_{ac} values with a fixed V_{dc} value (15 V). Response amplitude and phase as a function of swept frequency.

$$m\ddot{x} + c\dot{x} + kx + k_3x^3 = F\cos(\omega t), \tag{1}$$

where m, c, k, k_3, and F are the effective mass, damping coefficient, linear mechanical stiffness, cubic mechanical stiffness, and amplitude of actuation force, respectively. In the closed loop model, the right-hand side of the equation becomes $F_0\cos(\phi + \phi_0)$, where F_0, ϕ, and ϕ_0 are the self-sustaining force, instant phase, and phase delay, respectively. With the synchronization signal injected, the term of $F_s\cos(\omega_s t)$ is added as the perturbation, where F_s and ω_s are the perturbation force and frequency, respectively. Redefining time units ($t\sqrt{k/m} \to t$) and normalizing[23] Eq. (1) by the linear mechanical stiffness k lead to the following equation:

$$\ddot{x} + Q^{-1}\dot{x} + x + \beta x^3 = f_0\cos(\phi + \phi_0) + f_s\cos(\Omega_s t), \tag{2}$$

where $Q = \frac{\sqrt{km}}{c}$ denotes the quality factor, $\beta = \frac{k_3}{k}, f_0 = \frac{F_0}{k}, f_s = \frac{F_s}{k}$, and $\Omega_s = \frac{\omega_s}{\sqrt{k/m}}$ is the normalized perturbation frequency slightly larger than 1. Without the external perturbation, the analytical solution can be solved using the harmonic approach.[23] The harmonic solution $x(t) = A_0\cos\phi = A_0\cos(\Omega_0 t)$ can be obtained with a higher order harmonic term approximated as $\cos^3(\phi) \approx 3/4\cos(\phi)$.[22] With the solution being substituted into Eq. (2), we have

$$A_0 = \frac{Qf_0\sin(\phi_0)}{\Omega_0}, \tag{3}$$

$$\Omega_0^2 - \Omega_0^4 + \frac{3}{4}\beta Q^2 f_0^2 \sin^2\phi_0 - \frac{\Omega_0^3}{Q\tan\phi_0} = 0. \tag{4}$$

In the case of $\cot\phi_0 \cdot \Omega_0^3 \ll Q$, the solution of Eq. (4) can be obtained as

$$\Omega_0 = \frac{1}{\sqrt{2}}\left[1 + \left(1 + 3\beta Q^2 f_0^2 \sin^2\phi_0\right)^{1/2}\right]^{1/2}. \tag{5}$$

After being injected with a small perturbation f_s, the solution can be assumed to have the form $x(t) = A_s\cos\phi = A_s\cos(\Omega_s t - \phi_s)$, since the oscillation frequency is the same as the external perturbation in the synchronization regime. By separating the terms proportional to $\cos\Omega_s t$ and $\sin\Omega_s t$ and writing the complex form, we have

$$\begin{aligned}(1-\Omega_s^2)A_s + \frac{3}{4}\beta A_s^3 - f_0\cos(\phi_0) + i\left(f_0\sin(\phi_0) - \frac{\Omega A_s}{Q}\right)\\ = f_s\exp(-i\phi_s).\end{aligned} \tag{6}$$

For a small perturbation f_s, the solutions of Ω_s and A_s are close to those of Ω_0 and A_0, respectively.[23] Introducing the small perturbation parameter $\varepsilon = f_s/f_0$, we write

$$\Omega_s = \Omega_0 + \varepsilon\delta\Omega, A_s = A_0 + \varepsilon\delta A. \tag{7}$$

Substituting Eq. (7) into Eq. (6), by neglecting higher order terms, Eq. (6) becomes

$$\begin{aligned}\left(\frac{3Q\beta A_0\sin\phi_0}{2\Omega_0} + f_0\cos\phi_0 - \frac{i}{A_0}\right)\delta A\\ - \left(2Q\sin\phi_0 + \frac{i}{\Omega_0}\right)\delta\Omega = \exp(-i\phi_s).\end{aligned} \tag{8}$$

For the solvable condition of δA for a given value $\delta\Omega$, we thus have the predicate condition

$$\begin{aligned}\left(\frac{3Q\beta A_0^2\sin\phi_0}{2\Omega^2} + \frac{f_0 A_0\cos\phi_0}{\Omega} + 2Q\sin\phi_0\right)^2\delta\Omega^2\\ \le 1 + \left(\frac{3Q\beta A_0^2\sin\phi_0}{2\Omega_0} + f_0 A_0\cos\phi_0\right)^2.\end{aligned} \tag{9}$$

The condition given in Eq. (9) limits the values of $\delta\Omega_r$ to a critical interval $[-\delta\Omega_r, \delta\Omega_r]$. Then, the synchronization region can be obtained as $\Omega_0 - \varepsilon\delta\Omega_r \le \Omega_s \le \Omega_0 + \varepsilon\delta\Omega_r$. To find the quantitative value of $\delta\Omega_r$ in Eq. (9), we extract the oscillation parameters from the open loop tests. The natural frequency is $2\pi \times 208\,070$ Hz. The amplitude of the oscillation is scaled to be expressed by voltage. In Eq. (2), $f_0 = 3.29\,\mu$V and $\beta = 4.88\,\mathrm{V}^{-2}$. The two dashed lines in Fig. 3(a) show the calculated synchronization region as a function of phase delay from 40° to 90°. The dashed line in Fig. 3(b) shows that the location of the region can be shifted from 208 588 Hz to 209 460 Hz up and down depending on the value of phase delay. The size of the analytical synchronization region remains the largest when ϕ_0 equals $\pi/2$ as shown in Fig. 3(b).

The closed loop experiments are performed to verify the relationship between the synchronization region and phase delay. To facilitate the experiments on the effect of phase delay, we utilize the LIA with built-in PLL, consisting of a phase detector, tunable phase delay, and amplitude controlled output, to directly tune the value of ϕ_0 with the

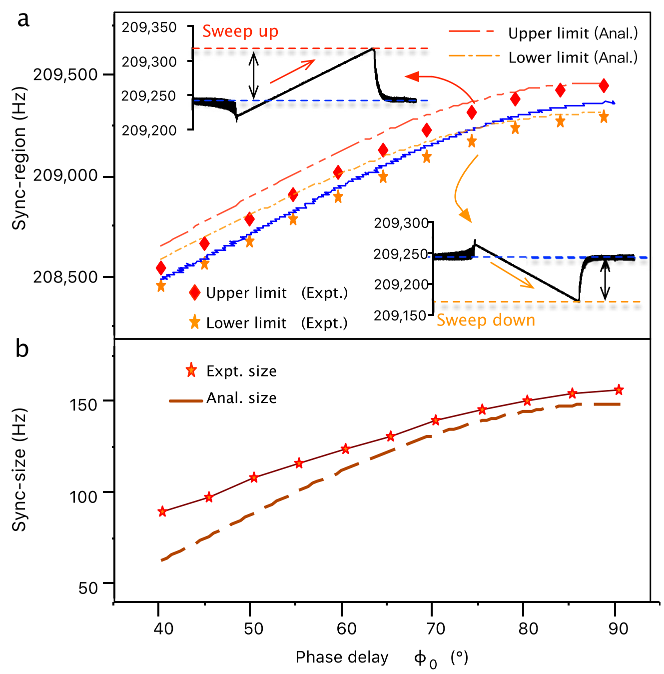

FIG. 3. Analytical and experimental results of the synchronization region. (a) Synchronization region as a function of phase delay. The blue dots show the self-oscillation frequency. The inset graphs show the up-sweeping and down-sweeping of the selected experimental operation points. (b) The size of the synchronization region as a function of phase delay. The stars and dashed line present the experiments and analytical results, respectively.

exciting voltage V_{ac} and bias voltage V_{dc} fixed on 400 mV and 15 V, respectively. The oscillation frequency, amplitude, and phase can be read out simultaneously. The correspondence between oscillation frequency and tuned phase delay can thus be obtained. The synchronization perturbation is generated by a function generator (Agilent 33250A) fixed on 10 mV injected with the self-sustaining force driving the resonator. The perturbation frequency is swept up and down in the vicinity of the oscillation frequency to find the synchronization region in which the oscillation frequency is locked to perturbation frequency. In upward sweeping, the oscillation frequency is suddenly entrained by the perturbation and goes up along with the perturbation frequency until desynchronization happens at Ω_u while desynchronizing at Ω_l in the downward sweeping case. We plot the measured synchronization boundary and between which, the red diamonds and the orange stars, the region lies as shown in Fig. 3(a). Figure 3(b) shows the synchronization region $\Omega_u - \Omega_l$ as a function of phase delay. We observed that the location of the synchronization region shifts and the size of the synchronization region varies depending on the phase delay. To have a better insight into these operation points, numerical results are shown in Fig. 4. The bifurcation diagram is obtained based on Eq. (2) with the unperturbed case considered ($f_s = 0$) using MatCont.[28] With the phase delay changing from 20° to 90° in steps of 5° shown as the red dots, the corresponding upper and lower synchronization boundaries are depicted (the short bars near the red dots) under 400 mV V_{ac} excitation (the dashed line). The inset picture in Fig. 4 indicates that the operation points move from 30° to 90°. For each

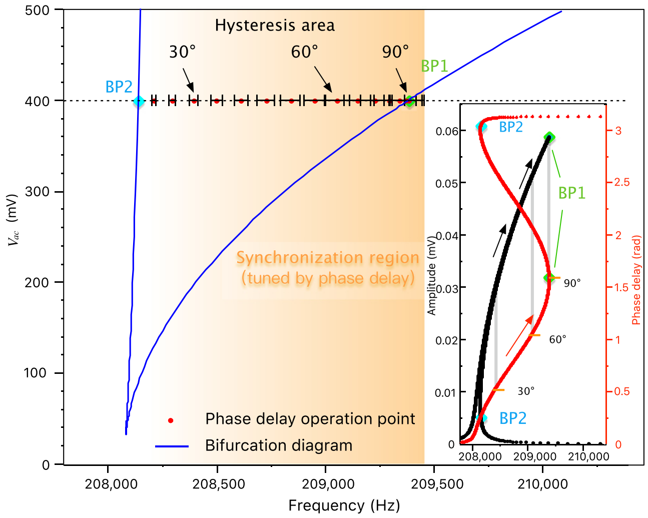

FIG. 4. Bifurcation diagram (blue line) and phase delay operation points (red dots) with the corresponding synchronization region (black bars) of the nonlinear oscillator. The inset graph shows the corresponding amplitude and phase branches of the response of the oscillator. The two bifurcation points (BP1 and BP2) are indicated. The colored area demonstrates the achievable synchronization region obtained by tuning phase delay.

phase delay operation point, the synchronization region size might be small (from 50 to 150 Hz) as shown in Fig. 3 and the small bar in Fig. 4. Nevertheless, the region can be expanded to the hysteresis area with continuous tuned phase delay for approximately 10 times enhancement, as shown in the colored area in the case of 400 mV ac excitation. To obtain an analytical expression of the synchronization range with phase delay, we solved Eq. (4) approximately under assumption $\cot\phi_0\Omega_0^3 \ll Q$. For a relatively small phase delay, this could bring some error; however, for a large phase delay ϕ_0, $\cot\phi_0$ approaches 0, and the prediction is accurate enough.

In addition, the effects of phase delay on the frequency stability are studied evaluated by Allan deviation.[29] The oscillation signals are logged out by a frequency counter after being filtered by a LPF shown in Fig. 1 with the self-oscillation driving condition remaining unchanged. Figure 5 shows the Allan deviation of the oscillation frequency measured for 300 s with a sample time of 0.1 s in the two cases of before synchronization and after synchronization. We can find that in the unsynchronized case, the oscillation is more stable when the phase delay ϕ_0 is $\pi/2$, which is in agreement with those in Refs. 30 and 31, as shown by the black dotted-line in Fig. 5(a). As ϕ_0 goes away from $\pi/2$, the frequency stability decreases up to half order from 180 ppb to 1094 ppb at 5 s (integration time). Once the oscillator is synchronized to the external perturbation, all of the frequency stability is improved to the same level (less than 100 ppb), as shown in Fig. 5(b). These results imply that phase delay affects the self-sustained oscillation on frequency stability, and this effect can be suppressed after synchronization. Figure 6 makes a more straightforward comparison of the frequency stability of different phase delays under various conditions based on the value of Allan deviation at a 1 s integration time. The circle dots with solid lines and the square dots with dashed lines depict the cases of before synchronization and after

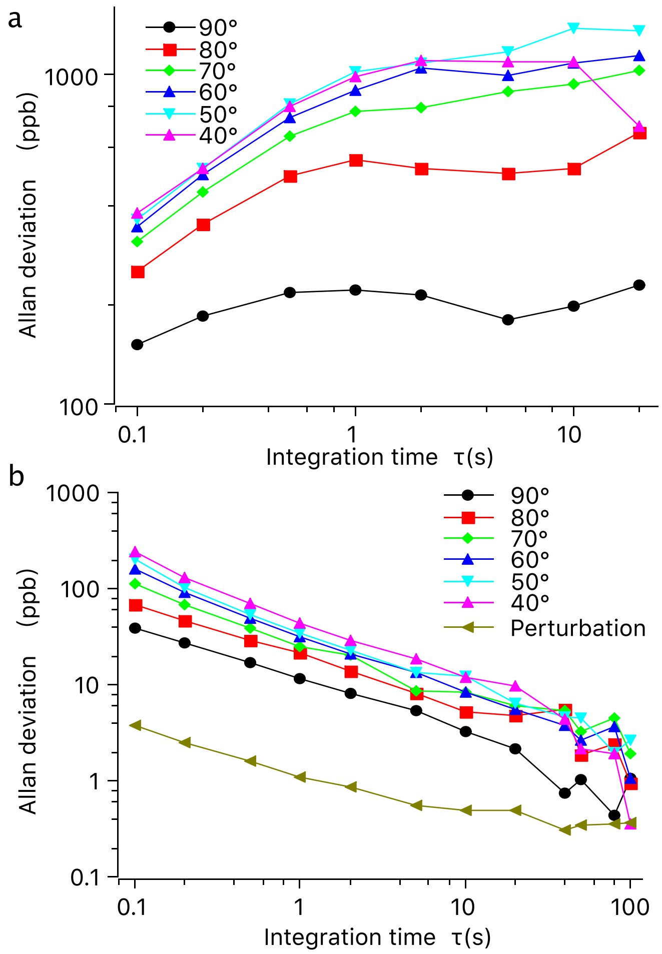

FIG. 5. Allan deviation of the oscillation frequency with the phase delay ranging from 40° to 90°. (a) Frequency stability without synchronization. (b) Frequency stability under synchronization. Dark yellow represents the frequency stability of the perturbation from the function generator.

synchronization, respectively. Under each V_{ac} excitation [Fig. 6(a)], the unsynchronized oscillator performs best while phase delay equals 90° (the bifurcation point BP1). After synchronization, the performance in each case is promoted to the same level. As shown in Eq. (3), phase delay affects the oscillation amplitude. To separate the amplitude effect, the Allan deviations at 1 s of various V_{ac} values (200, 255, 310, and 380 mV) with a fixed phase delay of 90° and the corresponding various phase delays (30°, 40°, 50°, 60°, 70°) with V_{ac} fixed at 400 mV for the same amplitude are directly compared in Fig. 6(b). The blue dots with solid lines show the frequency instability brought by nonlinear oscillation with V_{ac} and amplitude increasing. Differences of Allan deviation at 1 s between each corresponding red dot and blue dot uncover that even for the same amplitude, the phase delay would bring more frequency instability. Yet after synchronization, the frequency stability can be improved to the same level [the dashed lines in Fig. 6(b)].

In conclusion, the synchronization region is measured when the feedback phase delay was directly tuned, and the results reveal the

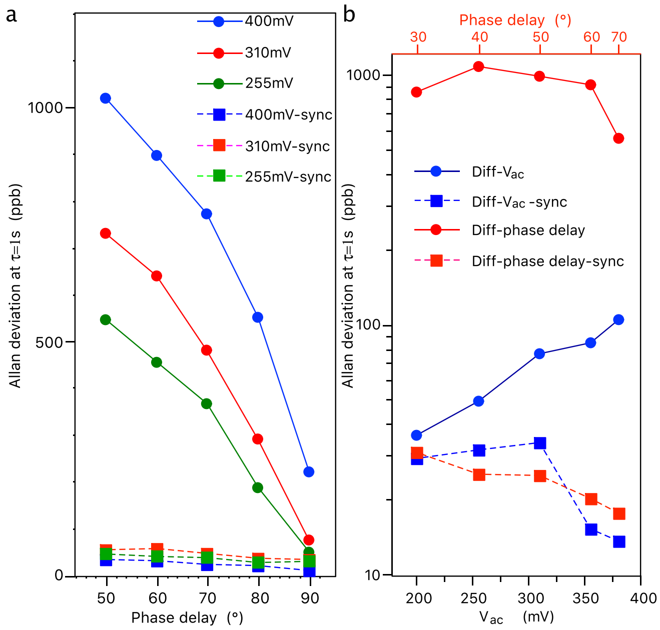

FIG. 6. Comparisons of Allan deviation under different phase feedback conditions. (a) The self-sustained oscillation outputs under various ac excitations with phase delay tuned from 50° to 90°. (b) Direct contrasts on the effects of phase delay and amplitudes on the frequency stability.

effects of phase delay on synchronization that the location of the synchronization region can be shifted, its size varies depending on the value of phase delay, and the frequency stability can be improved and maintains the same level after synchronization. This work bridges the synchronization region with the hysteresis area in nonlinear oscillators and provides an easy-to-implement approach for tuning the synchronization region, which makes it easier for synchronizing two oscillators to overcome the microfabrication error or even the narrow synchronization region of high order synchronization. In our experiments, the synchronization region can be easily tuned up to several kilohertz (for 10 times enhancement), which would highly lower the difficulty to implement synchronization.

This work was financially supported by the National Key R & D Program of China (No. 2018YFB2002303), National Natural Science Foundation of China (Nos. 51575439, 11621062, 11772293, and 11432012), Key Research and Development Program of Shaanxi Province (No. 2018ZDCXL-GY-02-03), and 111 Project (No. B12016). We also appreciate the support from the State Key Laboratory of applied optics and International Joint Laboratory for Micro/Nano Manufacturing and Measurement Technologies.

REFERENCES

[1] J. T. Van Beek and R. Puers, J. Micromech. Microeng. **22**, 013001 (2012).
[2] L. G. Villanueva, R. B. Karabalin, M. H. Matheny, E. Kenig, M. C. Cross, and M. L. Roukes, Nano Lett. **11**, 5054 (2011).
[3] K. L. Ekinci, X. M. H. Huang, and M. L. Roukes, Appl. Phys. Lett. **84**, 4469 (2004).
[4] D. Antonio, D. H. Zanette, and D. López, Nat. Commun. **3**, 806 (2012).
[5] L. G. Villanueva, E. Kenig, R. B. Karabalin, M. H. Matheny, R. Lifshitz, M. C. Cross, and M. L. Roukes, Phys. Rev. Lett. **110**, 177208 (2013).
[6] M. Sansa, E. Sage, E. C. Bullard, M. Gély, T. Alava, E. Colinet, A. K. Naik, L. G. Villanueva, L. Duraffourg, and M. L. Roukes *et al.* Nat. Nanotechnol. **11**, 552 (2016).
[7] L. G. Villanueva, R. B. Karabalin, M. H. Matheny, D. Chi, J. E. Sader, and M. L. Roukes, Phys. Rev. B: Condens. Matter Mater. Phys. **87**, 024304 (2013).
[8] M. Li, H. X. Tang, and M. L. Roukes, Nat. Nanotechnol. **2**, 114 (2007).
[9] S. K. Roy, V. T. K. Sauer, J. N. Westwood-Bachman, A. Venkatasubramanian, and W. K. Hiebert, Science **360**, eaar5220 (2018).
[10] Y. Huang, J. Wu, J. G. F. Flores, M. Yu, D. L. Kwong, G. Wen, and C. W. Wong, Appl. Phys. Lett. **110**, 111107 (2017).
[11] M. C. Cross, Phys. Rev. E **85**, 046214 (2012).
[12] J. K. Jang, A. Klenner, X. Ji, Y. Okawachi, M. Lipson, and A. L. Gaeta, Nat. Photonics **12**, 688–693 (2018).
[13] C. Huygens, *Christiaan Huygens' the Pendulum Clock, or, Geometrical Demonstrations Concerning the Motion of Pendula as Applied to Clocks* (Iowa State Press, 1986).
[14] A. Pikovsky, M. Rosenblum, and J. Kurths, *Synchronization: A Universal Concept in Nonlinear Sciences* (Cambridge University Press, 2003), Vol. 12.
[15] D. K. Agrawal, J. Woodhouse, and A. A. Seshia, Phys. Rev. Lett. **111**, 84101 (2013).
[16] D. Pu, R. Huan, and X. Wei, AIP Adv. **7**, 035204 (2017).
[17] D. Pu, X. Wei, L. Xu, Z. Jiang, and R. Huan, Appl. Phys. Lett. **112**, 013503 (2018).
[18] M. H. Matheny, M. Grau, L. G. Villanueva, R. B. Karabalin, M. C. Cross, and M. L. Roukes, Phys. Rev. Lett. **112**, 14101 (2014).
[19] F. Torres, A. Uranga, M. Riverola, G. Sobreviela, and N. Barniol, Sensors (Switzerland) **16**(10), 1690 (2016).
[20] P. Taheri-Tehrani, A. Guerrieri, M. Defoort, A. Frangi, and D. A. Horsley, Appl. Phys. Lett. **111**, 183505 (2017).
[21] O. Shoshani and S. W. Shaw, IEEE Trans. Circuits Syst. I **63**, 1 (2016).
[22] A. H. Nayfeh and D. T. Mook, *Nonlinear Oscillations* (John Wiley & Sons, 2008).
[23] D. Antonio, D. A. Czaplewski, J. R. Guest, D. Lopez, S. I. Arroyo, and D. H. Zanette, Phys. Rev. Lett. **114**, 34103 (2015).
[24] P. Taheri-Tehrani, M. Defoort, and D. A. Horsley, Appl. Phys. Lett. **111**, 183503 (2017).
[25] B. Yurke, D. S. Greywall, A. N. Pargellis, P. A. Busch, A. B. Laboratories, and M. Hill, Phys. Rev. A **51**, 4211 (1995).
[26] S. I. Arroyo and D. H. Zanette, Phys. Rev. E **87**, 052910 (2013).
[27] I. Kovacic and M. J. Brennan, *The Duffing Equation: Nonlinear Oscillators and Their Behaviour* (John Wiley & Sons, 2011), p. 369.
[28] A. Dhooge, W. Govaerts, and Y. A. Kuznetsov, ACM Trans. Math. Software **29**, 141 (2003).
[29] E. Rubiola, *Phase Noise and Frequency Stability in Oscillators* (Cambridge University Press, 2009).
[30] C. Zhao, G. Sobreviela, M. Pandit, S. Du, X. Zou, and A. Seshia, J. Microelectromech. Syst. **26**, 1196 (2017).
[31] G. Sobreviela, C. Zhao, M. Pandit, C. Do, S. Du, X. Zou, and A. Seshia, J. Microelectromech. Syst. **26**, 1189 (2017).